A method for the determination of the hydraulic properties of soil from MODIS surface temperature for use in land-surface models

Ethan D. Gutmann[1] and Eric E. Small[2]

Received 14 May 2009; revised 22 January 2010; accepted 29 January 2010; published 23 June 2010.

[1] Soil hydraulic properties (SHPs) play an important role in land-surface models, but their spatial distribution is poorly known, and it is not feasible to make field measurements of SHPs everywhere they are needed. In addition, the scale SHPs are measured on (10 cm) is substantially smaller than the scale at which land-surface models are run (>1 km). As a result, land-surface models need landscape hydraulic properties (LHPs), not SHPs. We present a method for identifying LHPs from MODIS surface temperatures. We calibrated LHPs in the Noah land-surface model using MODIS surface temperatures in 2005 at 14 sites from the Atmospheric Radiation Measurement Program (ARM) using locally observed forcing data from 2005. We then used observed flux data during this same time period for model verification. Next, we determined LHPs from MODIS surface temperature at five sites using High Resolution Land Data Assimilation forcing data from 2002. We then used these LHPS to run Noah with 2005 ARM forcing data and compared the output to the same observed 2005 fluxes. Fitting LHPs to MODIS data decreases the error in modeled latent heat flux from 98 W/m^2 to 67 W/m^2. Fitting LHPs to these same latent heat flux measurements decreases the error to 50 W/m^2. Therefore, two thirds of the parameter estimation improvement from calibration to in situ flux data can be achieved using remotely sensed surface temperature. These results are insensitive to errors in other parameters. For example, changing albedo by 0.1 changes the saturated conductivity (K_s) by 10% and the van Genuchten "m" parameter by 1%. However, changing minimum canopy resistance by 40 s/m produced a significant but mutually compensating change in both K_s and "m."

Citation: Gutmann, E. D., and E. E. Small (2010), A method for the determination of the hydraulic properties of soil from MODIS surface temperature for use in land-surface models, *Water Resour. Res.*, *46*, W06520, doi:10.1029/2009WR008203.

1. Introduction

[2] Soil hydraulic properties (SHPs) are an important component of land-surface models. SHPs control the movement of water in the soil, including infiltration and drainage rates. This, in turn, controls the surface and root zone soil moisture, which plays a critical role in the partitioning of available energy (net radiation minus ground heat flux) into evaporation and sensible heat flux. These fluxes are important in climate and weather forecasting [*Betts et al.*, 2003; *Koster et al.*, 2004], while the estimation of infiltration is important to flood forecasting and regional water balance modeling. In addition, *Seneviratne et al.* [2006] suggested that interactions between the land surface and the atmosphere may drive of much of the climatic variability predicted for Europe in the next 100 years.

[3] Current methods of estimating globally distributed SHPs for land-surface models are inaccurate [*Gutmann and Small*, 2005]. SHPs in land-surface models are commonly estimated based on the assumption that SHPs are related to soil texture [e.g., *Chen and Dudhia*, 2001; *Bonan et al.*, 2002; *Sellers et al.*, 1996]. Soil texture is commonly used because global maps of texture exist. However, soil texture has been shown to be a poor predictor of SHPs [*Soet and Stricker*, 2003; *Gutmann and Small*, 2005, 2007]. In addition, global soil texture maps are at a much coarser spatial resolution (e.g., 1°) [*Reynolds et al.* 1999] than the actual spatial variations in SHPs (often 10 s cm.)

[4] Because texture has been widely used, it is generally accepted as a proxy for SHPs, and most land-surface models expect the user to supply soil texture instead of SHPs [*Sellers et al.*, 1996; *Bonan et al.*, 2002; *Chen and Dudhia*, 2001]. This leads to studies such as that by *Santanello et al.* [2007] that attempt to predict soil texture from remotely sensed data instead of a more direct estimate of SHPs. Here, we propose that the land-surface modeling community consider moving away from this use of texture because it limits the variability of SHPs.

[5] Site-specific measurements of SHPs are difficult to make and are not made at a scale appropriate for use in land-surface models. SHPs are typically measured over a 100 cm^2 area either in the field [*Simunek and vanGenuchten*, 1997] or in the lab [*Vandam et al.*, 1992; *Stolte et al.*, 1994]. However, land-surface models are typically run with a single grid cell width of 1–100 km. As a result, different

[1]National Center for Atmospheric Research, Boulder, Colorado, USA.
[2]Department of Geological Sciences, University of Colorado at Boulder, Boulder, Colorado, USA.

0043-1397/10/2009WR008203

processes may influence the effective SHPs that should be used in land-surface models. Hereafter we will refer to effective SHPs as used in land-surface models as landscape hydraulic properties (LHPs).

[6] The effect of scale on hydraulic parameters has been recognized as an important factor by many authors [e.g., *Eching et al.*, 1994; *Zhu and Mohanty*, 2003; *Vrugt et al.*, 2004; *Duan et al.*, 2006]. Large-scale LHPs are influenced by processes not captured by small-scale measurements of SHPs. LHPs must account for the heterogeneity of SHPs within the region being modeled [*Zhu and Mohanty*, 2003], as well as the influences of variability in topography [*Stieglitz et al.*, 1997; *Stoeckli et al.*, 2007; *Bedford and Small*, 2008; *Kollet and Maxwell*, 2008] and vegetation [*Bonan et al.*, 1993; *Maayar and Chen*, 2006]. Heterogeneity of SHPs within a grid cell is important because of the nonlinear relationship between moisture content and hydraulic conductivity. This nonlinearity means that the average flux over an area with heterogenous SHPs will not be the same as the flux over an area with averaged SHPs [*Zhu and Mohanty*, 2003]. Topographic and vegetation heterogeneity exacerbate this problem by concentrating the inputs and outputs to and from the soil. Topography will result in water flowing to the low points and preferentially infiltrating in these locations. Vegetation heterogeneity will lead to more water removal via transpiration in locations with more vegetation. Additionally, soil flow processes not measured at small scales may be important. Soil water will preferentially flow through macropores [*Nachabe*, 1995] and flow will be modified by caliche cements or other local barriers to flow. This fits with recent results by *van Verseveld et al.* [2009], which suggested that vertical flow through the soil was probably dominated by preferential flow with little interaction between the water and the soil matrix.

[7] Because one cannot capture the large-scale response of a highly nonlinear system using the average of known small-scale parameters, it is necessary to derive large-scale parameters for the system at the scale of the model. Fortunately, a variety of data useful for land-surface modeling are measured at larger scales. For example, the footprint of a latent or sensible heat flux tower located 2 m above the ground is typically several hundred meters across, with a larger footprint for faster winds or higher towers. Additionally, satellites measure skin temperature at several spatial length scales from 60 m to 8 km. It is also possible to measure soil moisture from satellites at even larger scales (25 km). Other researchers have examined the possibility of determining LHPs from remotely sensed soil moisture [*Burke et al.*, 1998; *Santanello et al.*, 2007; *Pauwels et al.*, 2009]. We focus on the determination of LHPs from remotely sensed surface temperature because the scale of measurement is appropriate for current and future high-resolution weather forecasting and climate modeling (1–10 km) [e.g., *Leung et al.* 2006].

[8] Numerous researchers have used surface temperature to analyze surface hydraulic processes, but none have looked at incorporating surface temperature in an inverse framework to determine LHPs. *Boulet et al.* [2007] used a time series of surface temperature to analyze vegetation water stress and transpiration. Additionally, surface temperature has been used in conjunction with a vegetation index to infer soil moisture content [*Gillies and Carlson*, 1995]. This combination of surface temperature with a vegetation index has also been used to disaggregate low-resolution microwave soil moisture estimates [*Chauhan et al.*, 2003]. The surface temperature vegetation index combination has also been used to estimate evapotranspiration [*Friedl*, 1996], and other studies have used evapotranspiration to identify soil hydraulic properties [*Feddes et al.*, 1993]. However, nobody has combined these methods to determine SHPs from surface temperature, probably because the link between surface temperature and soil moisture or evapotranspiration is indirect. Surface temperature is controlled by many variables, including air temperature, solar radiation, past temperature, as well as soil moisture through its influence on latent heat flux/evapotranspiration (ET). Because there is no direct link between surface temperature and soil moisture, it is necessary to use an inverse procedure to estimate LHPs from MODIS surface temperature data.

[9] This paper will begin with a description of the Noah land-surface model, the data sets used in this study, and the inverse procedure itself. Then we will describe the three specific experiments we performed; first, an inverse modeling procedure with the best possible forcing data, second, an inverse procedure using potentially degraded forcing data that are available on a regional basis, and, finally, a sensitivity test to look at the effect of errors in other model parameters.

2. Methods

[10] We determined LHPs using an inverse procedure based on that of *Gutmann and Small* [2007], as described in section 2.7. We then performed three experiments to assess these LHPs. In the first experiment, we ran the inverse procedure at 14 sites (described in section 2.2) using observed forcing data from 2004–2005 to drive the Noah model (described in section 2.1) during the inverse procedure. The observed forcing data are as follows: 2 m air temperature, pressure and humidity, 10 m wind speed, and downward shortwave and longwave radiation. We verified these LHPs by comparing the model latent heat flux when using these LHPs to the observed latent heat fluxes from 2005. In the second experiment, we ran the inverse procedure at 5 of these sites for which we had High Resolution Land Data Assimilation System (HRLDAS) [*Chen et al.*, 2007] forcing data (described in section 2.5) to drive the model. For this experiment we spun up the model in 2001 and used 2002 for calibration, and we verified these LHPs by spinning up the model with observed forcing in 2004 and verifying with the same observed flux data from 2005 that were used in the first experiment. During this verification we ran the model using observed forcing data for the ARM sites to maintain consistency between the observed verification data and the model forcing. For the third experiment, we tested the sensitivity of the inverse procedure by running it after adding errors to the albedo, minimum canopy resistance, and roughness length at one site. We then present both the model output fluxes and derived LHPs as a function of the errors in these model parameters.

2.1. Noah Model

[11] In this study, we used the Noah land-surface model [*Chen and Dudhia*, 2001; *Ek et al.*, 2003]. The Noah land-surface model is a one-dimensional model that calculates

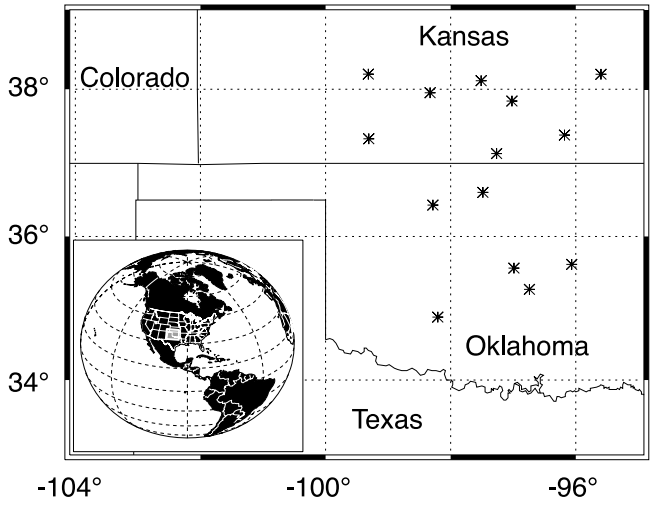

Figure 1. Map of ARM extended facilities used in this study.

the flow of heat and moisture vertically within a multilayer soil column and the exchange of heat and moisture to and from the atmosphere. We used eight soil layers with a 5 cm thick surface layer and layer thicknesses increasing to a 0.75 m bottom layer for a total soil column 2 m thick. The soil hydraulic component of the model solves the diffusion form of the Richards equation in one dimension (vertical) and we used the *van Genuchten* [1980] model for the relation between hydraulic head, moisture content, and hydraulic conductivity, as in *Gutmann and Small* [2007] (equations (1) and (2)).

$$\psi(\theta) = \left(S^{-\frac{1}{m}} - 1\right)^{\frac{1}{n}}/\alpha \tag{1}$$

$$K(\theta) = K_s S^{0.5}\left(1 - \left[1 - S^{\frac{1}{m}}\right]^m\right)^2, \tag{2}$$

where $\psi(\theta)$ is the water potential as a function of moisture content and $K(\theta)$ is the hydraulic conductivity as a function of moisture content, $S = \frac{\theta-\theta_r}{\theta_s-\theta_r}$. The fundamental soil hydraulic property parameters then are θ, the soil moisture content, θ_r, the residual moisture content, θ_s, the saturated moisture content, K_s, the saturated hydraulic conductivity, and α, n, and m, the curve fitting parameters related to the pore size distribution. The parameter space for this model is commonly limited by setting $m = 1 - \frac{1}{n}$, and we also adopt this convention. It should be noted that the residual moisture content is the moisture content at which water ceases to flow through the soil, except by vapor diffusion, and is lower than the wilting point.

[12] The fluxes from the land surface to the atmosphere are determined to conserve both mass and energy based on a Penman-Monteith type combination equation. The Noah model limits the latent heat flux with a canopy resistance term which it calculates as a function of the minimum canopy resistance divided by the leaf area index (LAI) and four functions that vary from zero to 1. The first three of these functions are related to the solar radiation, vapor pressure deficit, and air temperature. The last function is related to the average soil moisture in the root zone weighted by layer thickness (equation (3)).

$$F = \sum_{i=1}^{n\text{root}}\left(\frac{dz_i}{\text{root}_z} \times \frac{\theta_{\text{ref}} - \theta_i}{\theta_{\text{ref}} - \theta_w}\right), \tag{3}$$

where F is the factor canopy resistance is divided by to vary resistance as a function of soil moisture, dz_i is the thickness of layer i, root_z is the total thickness of the root zone, $n$root is the number of layers in the root zone, θ_w is the wilting point, below which plants are unable to transpire, θ_{ref} is the field capacity or reference water content above which soil water does not limit transpiration, and θ_i is the water content in layer i. θ_{ref} and θ_w are typically defined in the Noah land-surface model based on the soil hydraulic properties as in *Wetzel and Chang* [1987]. F is limited to fall between zero and one, inclusive. When the average soil moisture decreases, the total canopy resistance term increases, leading to a decrease in latent heat flux. For further information consult *Chen and Dudhia*, [2001] and *Jacquemin and Noilhan* [1990].

[13] The Noah model is designed to be coupled with the Weather Research and Forecasting model (WRF) or to be run in an offline mode in which it can use atmospheric boundary conditions measured near the ground surface. We used the offline mode here. In offline mode it requires air temperature, pressure, humidity, wind speed, shortwave and longwave downwelling radiation, and precipitation forcing data. The Noah model typically runs on a 30 min time step, but we shortened this to 3 min to improve stability for some of the more extreme SHP parameter sets.

[14] We initialized the model based on observed soil data when available, with a vertically homogenous moisture and temperature profile. We performed a simple sensitivity test by varying the initial moisture content and found it had very little impact on the inverse model results. In all cases, the model was spun up for 1 year prior to the start of the inverse procedure and verification procedure. While the deep soil moisture does not completely stabilize after the full 2 year model run, the changes are small after the first year, and the root zone soil moisture shows no significant changes as a function of initial moisture content after the initial spin up year.

2.2. ARM Sites

[15] We used 14 sites from the Atmospheric Radiation Measurement (ARM) program. The ARM sites are spread out across northern Oklahoma and southern Kansas (Figure 1). At these sites, the model forcing data are observed along with turbulent fluxes (latent and sensible heat). The turbulent fluxes are measured by the Bowen ratio method at 8 sites, and by the eddy covariance method at 7 sites. Table 1 summarizes the model parameters used for each site.

[16] The 14 ARM sites cover a range of annual precipitation levels and vegetation characteristics. These sites are all of the ARM extended facility sites in the Southern Great Plains region that have forcing and turbulent flux data for the period 2004–2005. Mean annual precipitation ranges from 580 mm/yr at site E1 to 970 mm/yr at site E7. Mean vegetation cover ranges from 10% grass cover at site E1 to 95% forest cover at site E21 and we varied the vegetation

Table 1. Site Parameters[a]

Site	Veg. Type	Veg. Fg	Root Depth	Txt. Cls.	MAP (mm)	Albedo	Z_o (m)	Lat.	Lon.
ARM E1	Wheat	10	55 cm	Si.L.	580	0.19	0.07	38.202	−99.316
ARM E3	Wheat	80	55 cm	Si.Cl.L.	910	0.20	0.07	38.201	−95.597
ARM E4	Grass	50	55 cm	L.Sa.	710	0.17	0.05	37.953	−98.329
ARM E5	Wheat	40	55 cm	Si.L.	760	0.19	0.07	38.114	−97.513
ARM E6	Alfalfa	70	55 cm	Si.Cl.L.	860	0.19	0.07	37.842	−97.020
ARM E7	Grass	75	55 cm	Si.L.	970	0.20	0.05	37.383	−96.180
ARM E8	Grass	30	55 cm	L.Sa.	620	0.18	0.05	37.333	−99.309
ARM E9	Grass	55	55 cm	L.	810	0.20	0.05	37.133	−97.266
ARM E13	Grass	35	55 cm	Si.L.	810	0.18	0.05	36.605	−97.485
ARM E15	Grass	50	55 cm	Sa.	710	0.19	0.05	36.431	−98.284
ARM E20	Grass	65	55 cm	L.	900	0.18	0.05	35.564	−96.988
ARM E21	Forest	95	125 cm	Si.L.	910	0.14	0.80	35.615	−96.065
ARM E24	Wheat	50	55 cm	Si.L.	790	0.17	0.07	34.883	−98.205
ARM E27	Grass	65	55 cm	L.	950	0.17	0.05	35.269	−96.740

[a]Abbreviations: Fg, fraction green vegetation cover; Txt. Cls., texture class; Sa., sand; L., loam, Si., silt; Cl., clay; MAP, mean annual precipitation; Z_o, surface roughness.

cover over the course of the model run based on the MODIS NDVI product as described below. The texture of the topsoil layer varied from site to site as follows: silt loam (E1,5,7,13,21,24), silty clay loam (E3,6), loamy sand (E4,8), loam (E9,20,27), and sand (E15). Other texture classes reported at each site were commonly the same or very similar to the top layer, with clay and clay loam present deeper in the soil column at several sites. No observations of land-surface roughness were available at these sites, so we used the Noah model's default value for the given land cover type. Albedo was derived from observations of downward and upward shortwave observations at each site and, at all sites, it is within 0.02 of the Noah default albedo for each land cover type.

[17] For these sites, we initialized the model soil moisture as dry (θ = 0.10) or wet (θ = 0.35) depending on observed values from heat dissipation probes from January of 2004. Although we can reasonably determine whether the soil is wet or dry from these data, more precise determination of initial soil moisture would be highly dependent on the calibration at the measurement location, which is imprecise. Sensitivity testing suggests that errors in the initial value would not substantially affect the results.

[18] At all sites, time varying vegetation cover was derived from MODIS observations. We compute the fraction of green vegetation cover (F_g) from the MODIS 16-day NDVI product using equation (4) as in *Gutman and Ignatov* [1998].

$$F_g = \frac{\mathrm{NDVI} - \mathrm{NDVI}_o}{\mathrm{NDVI}_\infty - \mathrm{NDVI}_o}. \tag{4}$$

[19] We use this formulation because it is the most widely used form in the land-surface modeling community and because historical NDVI data are available for retrospective studies while more modern vegetation measures such as the Enhanced Vegetation Index or EVI [*Huete et al.*, 1994] are not. We do not expect the fundamental conclusions of this study to be affected by the use of different vegetation indices. We used a value of 0.2 for NDVI_o consistent with observed soil NDVI [*Montandon and Small*, 2008]. We used a value of 0.85 for NDVI_∞ consistent with observed maximum NDVI in this region. We interpolated the 16-day product to the model time step using a cubic spline on temporally smoothed NDVI data. This time varying NDVI product inherently includes effects such as local crop harvest, and the natural spring green up at each site. While we do not include variations in surface roughness that may occur as part of this change in vegetation cover, the Noah model is not commonly run with time variant surface roughness. In the future this could be an area for model improvement.

2.3. Turbulent Fluxes and Closure

[20] Turbulent flux measurements can be imprecise, but closure of the energy balance can be used to constrain the flux measurements. Flux measurements made by the Bowen Ratio method inherently have a closure of 1. Although this does not mean they are perfect, it means that no simple correction is possible. The observed closure (equation (5)) of the surface energy balance from measured fluxes at the eddy covariance sites generally ranged from 0.8 to 1.2.

$$\mathrm{closure} = \frac{\mathrm{LH} + \mathrm{SH}}{R_n - G}, \tag{5}$$

where LH is latent heat flux, SH is sensible heat flux, R_n is net radiation, and G is ground heat flux. There is no storage term in this equation because the surface layer in Noah is infinitely thin. Ground head flux was not measured at these sites, so we used G from the default model simulations at each site. Because G is commonly less than 20% of the midday available energy and errors in modeled G are likely to be small [*Hogue et al.*, 2005], the use of model G is not expected to add much error to the final result. At the ARM sites, we found the average midday G to be 11% of R_n with at standard deviation of 7%.

[21] *Twine et al.* [2000] performed a rigourous study of eddy covariance measurements and energy balance and found that the eddy covariance was the largest source of error, typically underestimating fluxes by 10% to 30%. *Kurc and Small* [2004] found that the eddy covariance method sometimes underestimated fluxes by 10% relative to a co-located Bowen ratio station. They attributed this to closure problems. *Kabat et al.* [1997] found that average daily measurements with the two methods agreed well, but there was a lot of scatter in hourly comparisons. Part of these errors may stem from variations in the location the observed turbulent fluxes come from. The location varies as a func-

tion of boundary layer stability, wind speed, and wind direction. This variation can mean that fluxes derived from the eddy covariance method do not always match the local energy balance and thus have closure which deviates from 1. The Bowen ratio technique can also have problems related to fetch, but this technique forces closure on the fluxes so that no correction is possible.

[22] A closure value of 1 means that the observed turbulent heat fluxes balance the observed available energy. Deviations from a closure of 1 imply errors in the observations. Closure less than (greater than) 1 means that the observed turbulent fluxes are less than (greater than) the observed available energy. Periods in which closure was below 0.8 or above 1.2 were excluded from the analysis. Closure was never above 1.2 for a significant period. Errors in closure are likely to come from the measurement of LH and SH [*Twine et al.*, 2000]. To correct errors in closure, we adjusted the measured LH and SH at all sites to force closure while keeping the Bowen ratio constant as recommended by *Twine et al.* [2000] (equations (6) and (7)).

$$\mathrm{LH}^{*} = \mathrm{LH} + \mathrm{LH}\left(\frac{\overline{R_n} - \overline{G}}{\overline{\mathrm{LH}} + \overline{\mathrm{SH}}} - 1\right), \tag{6}$$

$$H^{*} = H + H\left(\frac{\overline{R_n} - \overline{G}}{\overline{\mathrm{LH}} + \overline{\mathrm{SH}}} - 1\right), \tag{7}$$

where LH* and SH* are the corrected latent and sensible heat fluxes, respectively, and $\overline{R_n}$, $\overline{G}$, $\overline{\mathrm{LH}}$, and $\overline{\mathrm{SH}}$ denote the midday mean value of each flux for the day of the current measurement. These fluxes were measured every 30 min, but closure was forced on a daily basis, not for the individual measurements. While this will not remove all of the error in the flux measurements, it makes them consistent with the radiation measurements that are supplied to the model as inputs. We did not want to force closure for each 30 min time step because we wanted to avoid influencing the data too much with modeled *G*.

2.4. Soils Database

[23] We used the SHP database of *Schaap and Leij* [1998] as the basis for the inverse procedure. This database is a collection of three other databases (RAWLS, AHUJA, and UNSODA), and as such it is one of the largest SHP databases available. The public domain UNSODA database [*Leij et al.*, 1996] forms the bulk of the *Schaap and Leij* [1998] database. The database of *Schaap and Leij* [1998] contains 1306 soils with complete SHP measurements. Only three soil texture classes are represented by fewer than 50 soils. We used this database because of its international nature, its availability to other researchers, and because it has been used extensively [*Leij et al.*, 1997; *Arya et al.*, 1999; *Hoffmann-Riem et al.*, 1999; *Poulsen et al.*, 2000; *Schaap et al.*, 2001]. The SHPs in this database were not measured within the LSM framework or at the LSM scale, but it is the best database available. It is based on lab and field measurements of relatively small soil samples that would cover an area of approximately 100 cm^2. These may show more variation in SHPs than would be seen in SHPs derived at the larger scales used in LSMs. However, these measurements also do not include large scale soil variation such as macropores that would be likely to increase the observed variation.

2.5. High Resolution Land Data Assimilation System Data

[24] A key aspect of this study is the use of forcing data from a regional data set in addition to local observations. This is important because it will be necessary to use a regional data set if we wish to map LHPs over a regional or global area. We use the 4 km gridded HRLDAS forcing data set [*Chen et al.*, 2007] because it has the highest spatial resolution of the available regional and global data sets. HRLDAS precipitation data come from the 4 km NCEP stage-IV rainfall product. These data are derived by merging gauged precipitation records with RADAR data. *Chen et al.* [2007] found that this precipitation product had a cumulative error of 10–20 mm over the 40 day record of the International H_2O Project (IHOP). The precipitation had a slightly negative bias (HRLDAS less than observed) at the drier, western IHOP sites, and the precipitation had a slightly positive bias at the wetter western IHOP sites. HRLDAS downward solar radiation product comes from the GOES hourly product. They also found that the solar radiation product had a midday root mean square error (RMSE) of 80 W/m^2, and overestimated solar radiation during the early morning and late afternoon. *Chen et al.* [2007] found that midday solar radiation generally had a slightly positive bias less than 20 W/m^2. HRLDAS downward longwave forcing data come from the NCEP Eta Data Assimilation (EDAS) product. Errors in longwave forcing were determined to be negligible relative to errors in solar radiation. Finally, HRLDAS surface wind, temperature, pressure, and humidity were derived from EDAS 40 km data. *Chen et al.* [2007] compared these data to 113 observation points from the Oklahoma Mesonet. They found RMSE values of <6 hPa for pressure, <2.2 K for temperature, <1.1 g/kg for mixing ratio, and roughly 1.4 m/s for wind speed. All of these variables had a small high (low) bias during the day (night).

2.6. MODIS Data

[25] We use the MOD11A1 (Terra) and MYD11A1 (Aqua) MODIS land-surface temperature (LST) version 4 1 km daily products from the Terra and Aqua satellites. These data are available at no cost from the NASA Warehouse Inventory Search Tool (WIST, https://wist.echo.nasa.gov/). Terra overpasses occur at 10:30 local time, while Aqua overpasses occur at 13:30 local time. These two passes provide a morning and afternoon observation. These two observations provide both a rate of heating through the day and a near maximum daily temperature. The exact local measurement time for each grid cell varies depending on ground position relative to the orbit ground track; grid points west of the satellite ground track are observed earlier relative to local sun time while grid points east of the satellite ground track are observed later. We used the local measurement time of each grid cell when determining which model time step to compare the MODIS data to. The nominal grid spacing of this data product is approximately 1 km (927 m), although the width of an individual observation will range up to 6 km at a view angle of 60° off nadir.

[26] These land-surface temperature observations have been verified to be accurate to better than 1 K [*Wan et al.*, 2004]. These data products use MODIS bands 31 (10.6–11.3 μm) and 32 (11.8–12.3 μm) with the generalized split window algorithm [*Wan and Dozier*, 1996]. In its simplest form, the split window algorithm assumes a known land-surface spectral emissivity and uses upwelling radiation measured in two spectral bands to solve for two unknowns (atmospheric emission and land-surface temperature). The MODIS LST product incorporates improvements to the split window algorithm based on the view angle, total column water content, and lower atmosphere temperatures [*Wan et al.*, 2004].

[27] We tested various subsets of the MODIS data based on the supplied quality assurance data but found that the inverse model was relatively unaffected and may have behaved worse when some data were removed. As a result, we used all data for which a LST was produced as part of the MOD11A1 and MYD11A1 products. We suspect that errors in the MODIS product are smaller than the errors related to comparing an imperfect model to a large, heterogenous, and changing land surface, for example, an individual MODIS LST observation may be 1 km across one day and 6 km across another day.

[28] Because the variation in the viewing angle of the satellite is large, we analyzed errors between MODIS LST and modeled LST as a function of view angle. There was a very slight relationship between sensor view angle and LST-model error, but we did not find any substantial improvement to the inverse procedure by limiting the view angles we used. We performed this same analysis to compare LST errors to the angle between the sensor view angle and the solar illumination angle. Similarly, we found no improvement to the inverse procedure by subsetting the angles used and only a slight correlation between errors and the sun-view angle.

2.7. Inverse Procedure

[29] The inverse procedure used in this study follows that of *Gutmann and Small* [2007] and is broken into two parts. First, we calibrated the Noah Co parameter to MODIS observations of surface temperature during dry days. Dry days were defined as days in which the model latent heat flux is less than 100 W/m^2. The Co parameter comes from *Zilitinkevich* [1995] and regulates turbulent heat fluxes. Co is used in equation (8) to calculate the roughness length for turbulent fluxes SH and LH.

$$z_{o-h} = z_o \exp\left(-\kappa \mathrm{Co}\sqrt{\frac{u^* z_o}{\nu}}\right), \tag{8}$$

where z_o is the standard roughness length for momentum, κ = 0.4 is the von Karman constant, ν is the kinematic molecular viscosity of air ($\approx 1.6 \times 10^{-5}$ m^2/s), u^* is the friction velocity, and Co is a calibration parameter set to 0.1 in Noah by default. The Co parameter was determined to be very important to the calculation of surface temperature by *Chen et al.* [1997] and land-surface atmosphere exchange by *LeMone et al.* [2008] and *LeMone et al.* [2009]. We calibrated Co with dry days because the model will be insensitive to LHPs during these periods.

[30] Second we calibrated the model LHPs to MODIS observations of surface temperature on days for which the model midday latent heat flux is greater than 100 W/m^2. To avoid problems related to transient cloud cover, we only used days in which the midday average solar radiation was greater than 600 W/m^2. Based on the inverse procedure in [*Gutmann and Small*, 2007], LHP calibration was performed by running the model once for each of the 1306 soils in the database of *Schaap and Leij* [1998]. We then selected the LHPs from the model run with the smallest error between modeled surface temperature and MODIS observations of surface temperature. Error was calculated as the root mean square (RMS) error between the set of MODIS observations and the corresponding model temperature. As in *Gutmann and Small* [2007], we also selected the optimal LHPs based on the observed energy fluxes ($\mathrm{LHP_{opt}}$), here error was calculated based on the midday average heat flux and the RMS value was calculated over all days. Finally we select the LHPs based on the soil texture class average SHPs at that site ($\mathrm{LHP_{txt}}$). The $\mathrm{LHP_{opt}}$ and $\mathrm{LHP_{txt}}$ models are used for reference as the best possible model and the current default model, respectively. We used the inverse model to perform three experiments as described below.

2.7.1. Experiment 1: ARM Forcing Data

[31] The first model experiment was designed to test the quality of LHPs derived from MODIS surface temperature when the forcing data are measured locally, thus minimizing errors. We ran the model for two years (2004–2005) at the 14 ARM sites with locally observed precipitation, air temperature, humidity, wind speed, pressure, and downward shortwave and longwave radiation. The first year of the model run was used to spin-up the model, and the second year was used in the inverse modeling procedure. The inverse modeling procedure was run once at each site using MODIS surface temperature for the objective function and ARM forcing data to drive the model ($\mathrm{LHP_{af}}$). We evaluated these results by comparing the model output latent and sensible heat fluxes to the observed fluxes for 2005.

2.7.2. Experiment 2: HRLDAS Forcing Data

[32] The second model experiment was designed to test the quality of the LHPs derived from MODIS surface temperature when no observations of local weather forcing are available, because this is how the inverse procedure would need to be run to map LHPs on a regional or global scale. In addition, this experiment tested LHPs calibrated for a time period (2002) other than the time period used for verification (2005). By using a different time period for calibration, we tested whether the derived LHPs are a function of the location or the calibration period. It also tests whether they are compensating for errors in the forcing data. In this experiment, we used the HRLDAS forcing data for precipitation, air temperature, humidity, wind speed, pressure, and downward shortwave and longwave radiation. We ran the model for 18 months (January 2001–June 2002). Again, we used the first year to spin-up the model. Then we used the 6 months in 2002 for the inverse modeling procedure. The inverse procedure was run once at each site using MODIS surface temperature for calibration and HRLDAS forcing data to drive the model ($\mathrm{LHP_{hf}}$). As in the first experiment, we evaluated these results by running the model with observed forcing data for 2004–2005 and comparing the modeled latent and sensible heat fluxes to the observed fluxes in 2005. We only used five sites in this experiment

Table 2. Parameters Used in Experiment 3 Sensitivity Tests

Site	Albedo	Z_o (m)	Stomatal Resistance (s/m)
ARM E9	0.10	0.05	40
ARM E9	0.14	0.05	40
ARM E9	0.17	0.05	40
ARM E9	0.19	0.05	40
ARM E9	0.20	0.05	40
ARM E9	0.21	0.05	40
ARM E9	0.23	0.05	40
ARM E9	0.26	0.05	40
ARM E9	0.20	.005	40
ARM E9	0.20	.01	40
ARM E9	0.20	.03	40
ARM E9	0.20	.04	40
ARM E9	0.20	.06	40
ARM E9	0.20	.07	40
ARM E9	0.20	.1	40
ARM E9	0.20	.5	40
ARM E15	0.18	0.05	30
ARM E15	0.18	0.05	35
ARM E15	0.18	0.05	40
ARM E15	0.18	0.05	45
ARM E15	0.18	0.05	50
ARM E15	0.18	0.05	55
ARM E15	0.18	0.05	60
ARM E15	0.18	0.05	65
ARM E15	0.18	0.05	70
ARM E15	0.18	0.05	75

because we only had HRLDAS forcing data for the ARM sites E7, 8, 9, 13, and 15.

2.7.3. Experiment 3: Model Sensitivity

[33] The third model experiment was designed to test the sensitivity of the inverse procedure to errors in other model parameters, such as surface roughness, albedo, and minimum canopy resistance. We selected these parameters because we believed them to be the most important remaining parameters in the land-surface model because they cover the three other most important processes, radiation energy balance, atmospheric exchange, and vegetation effects. *Bastidas et al.* [1999] studied the sensitivity of a land-surface model to various model parameters and found that minimum canopy resistance was the most important vegetation parameter, and surface roughness was shown to be equally important.

[34] To perform this test, we used the same set up as in experiment 1 at ARM site E9, but we varied albedo from 0.1 to 0.26 (observed = 0.2). For reference, the default albedo for an evergreen broadleaf forest is 0.1, and for a playa it is 0.3. We varied albedo in small increments near the observed value because small errors are more likely, we then included a wider range of values to cover a reasonable range of land-surface values. It should be noted that because albedo can be reasonably determined from satellite observations, such large errors in a real model are highly unlikely.

[35] We perform this same experiment with surface roughness length ranging from 0.005 m to 0.5 m (default = 0.05 m). The default roughness for water or snow is 0.001 m and for forests it is around 0.8 m. Because of the large range of possible values, we varied roughness on a log scale for the more extreme values and linearly near the default value to provide more detail for more likely values.

[36] Finally, we perform this experiment at site E15 with minimum canopy resistance ranging from 20 s/m to 75 s/m (default = 40 s/m). The default minimum canopy resistance for a grass is 40 s/m, and for a savanna or cropland/woodland mosaic it is 70 s/m. We varied minimum canopy resistance linearly over this range.

[37] These ranges were selected to cover almost the entire range of expected natural values. We believe it is reasonable to assume that some amount of information is available about a site ahead of time (e.g., is it a forest or a lake) thus we did not believe it was not necessary to test the entire range. All of the parameters used in this experiment are summarized in Table 2.

[38] We selected ARM site E9 and 15 because the model performed well in the previous experiments at these sites and because they have intermediate values for vegetation cover and mean annual precipitation. As in experiment 1, we evaluate these results by comparing the model output latent and sensible heat fluxes to the observed fluxes for 2005. Additionally, we look at the variation of LHPs as a function of errors in each model parameter. We compare these variations to the distribution of SHPs in the database of *Schaap and Leij* [1998], and to the LHP_{opt} and LHP_{txt} values.

3. Results and Discussion

[39] We quantify how well our inverse procedure improved the representation of the land-surface hydrology by calculating the RMSE and bias between the midday measured and modeled latent and sensible heat fluxes. We also present the coefficient of determination between measured and modeled latent heat flux. We focus on the latent heat flux because this flux is more sensitive to SHPs than is the sensible heat flux [*Bastidas et al.*, 1999]. We compare the Noah land-surface model output using the experimental LHPs, LHP_{opt}, and LHP_{txt}. The optimal model error represents the combined error due to errors in model physics, model structure, other model parameters, observed forcing, and observed fluxes. The optimal model error therefore represents the minimum error the model is capable of when only LHPs are calibrated. The texture model error is presented to show how well the Noah model performs when using the default hydraulic properties.

[40] As examples, ARM sites E9 and E15 are presented in Figures 2 and 3, respectively. Regardless of LHPs used, the simulated time series follow the trends of increasing (decreasing) ET (sensible heat flux) associated with rain events. At ARM site E9 (Figure 2), the texture modeled ET decreases more rapidly from day 170 to day 220 and from day 240 to day 270 compared to the observed ET and compared to the optimal and experimental models. This may be due to the substantially higher surface runoff predicted by the texture model.

[41] At ARM site E15 (Figure 3), the texture modeled ET is consistently lower than the observed ET and ET from all of the calibrated LHP model runs. This is due to a much higher saturated conductivity that causes all of the water to drain past the bottom of the root zone, resulting in high subsurface runoff. Additionally, Figure 3 illustrates the potential problems resulting from errors in forcing data. In this extreme case, several rainstorms appear to be missing from the forcing data around day 180–200. As a result, the observed ET is much higher than the modeled ET. We removed the period from day 180 to day 225 from both the

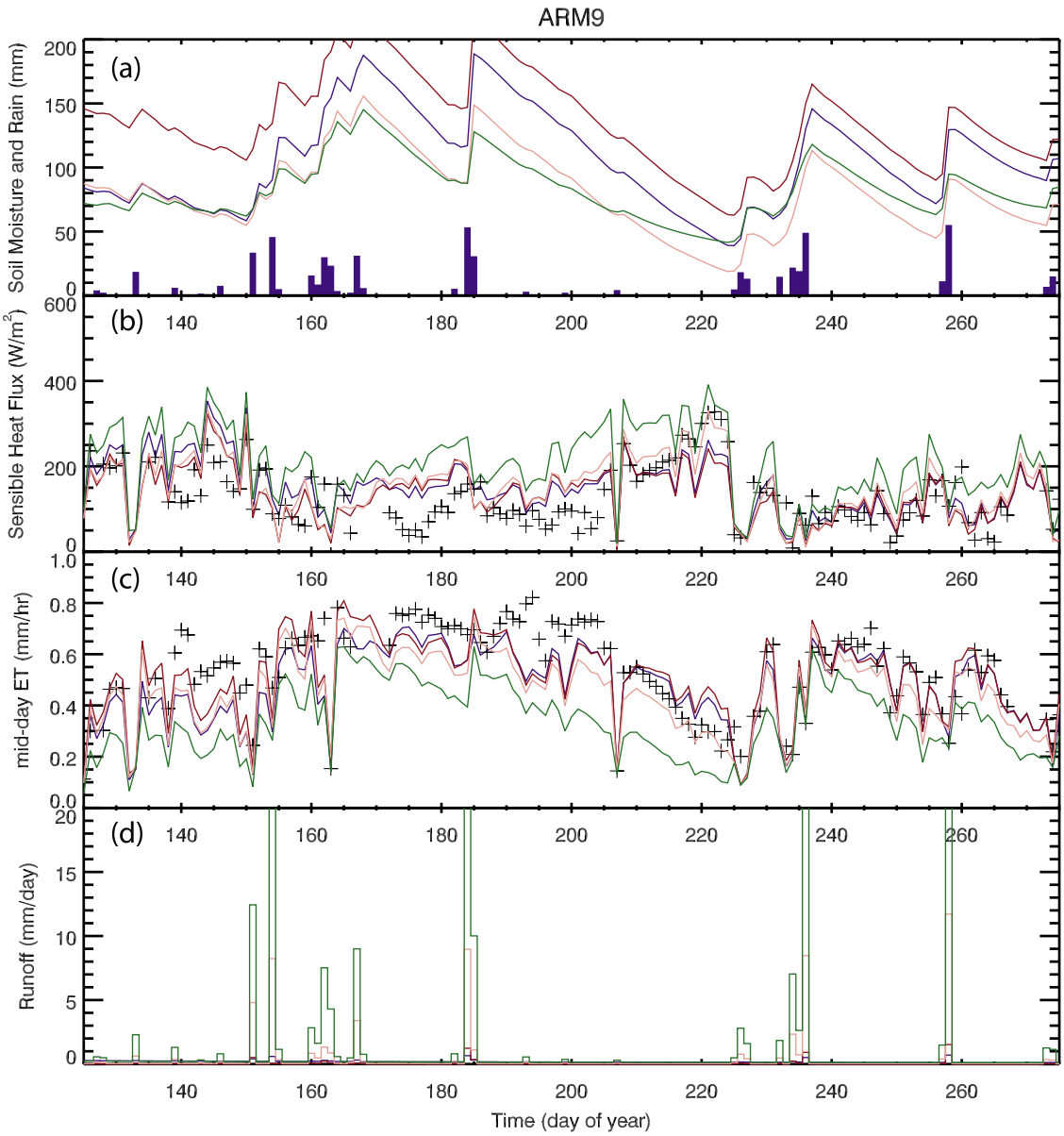

Figure 2. Site details for ARM site E9. (a) Soil column water content and daily precipitation, (b) midday sensible heat flux, (c) midday ET, and (d) combined surface and subsurface runoff, for the (blue online, thick black in print) LHP_{opt}, (red online, thick gray in print) LHP_{af}, (light red online, thin gray in print) LHP_{hf}, (green online, thin black in print) LHP_{txt}, and observations (+).

verification and calibration procedures. This was the largest error in the forcing data that we observed. The other periods we removed from analysis were days 225–260 as site E20, and days 196–206 at site E21.

3.1. Experiment 1: ARM Forcing Data

[42] Results for experiment one are presented in Table 3 and Figures 4 and 5. We summarize the data for the 10 sites that had an LH error less than 70 W/m^2 in the optimal model. These sites are E3, 4, 6, 7, 8, 9, 15, 20, 24, and 27. We removed the remaining sites (E1, 5, 13, and 21) because if the optimal model is unable to reasonably fit the observed surface fluxes, it is likely that the observed forcing and fluxes are inconsistent at these sites, or that errors in other model parameters or errors in model structure dominate; as such the results below are the best case results. We also present the summary for all sites at the bottom of Table 3, while these results are less pronounced, they are very similar to those presented below.

[43] The optimal model performs the best, but the MODIS-derived model reduces error by 65% relative to the texture and optimal models and the MODIS-derived model reduces 90% of the cumulative bias. The average LH error for the MODIS-derived model was 67 W/m^2 and the bias was −6.4 W/m^2. The average LH error for the optimal model was 50.4 W/m^2 and the bias was −0.9 W/m^2. The average LH error for the texture model was 97.8 W/m^2 and the bias was −50.2 W/m^2. Despite the low cumulative bias, the bias

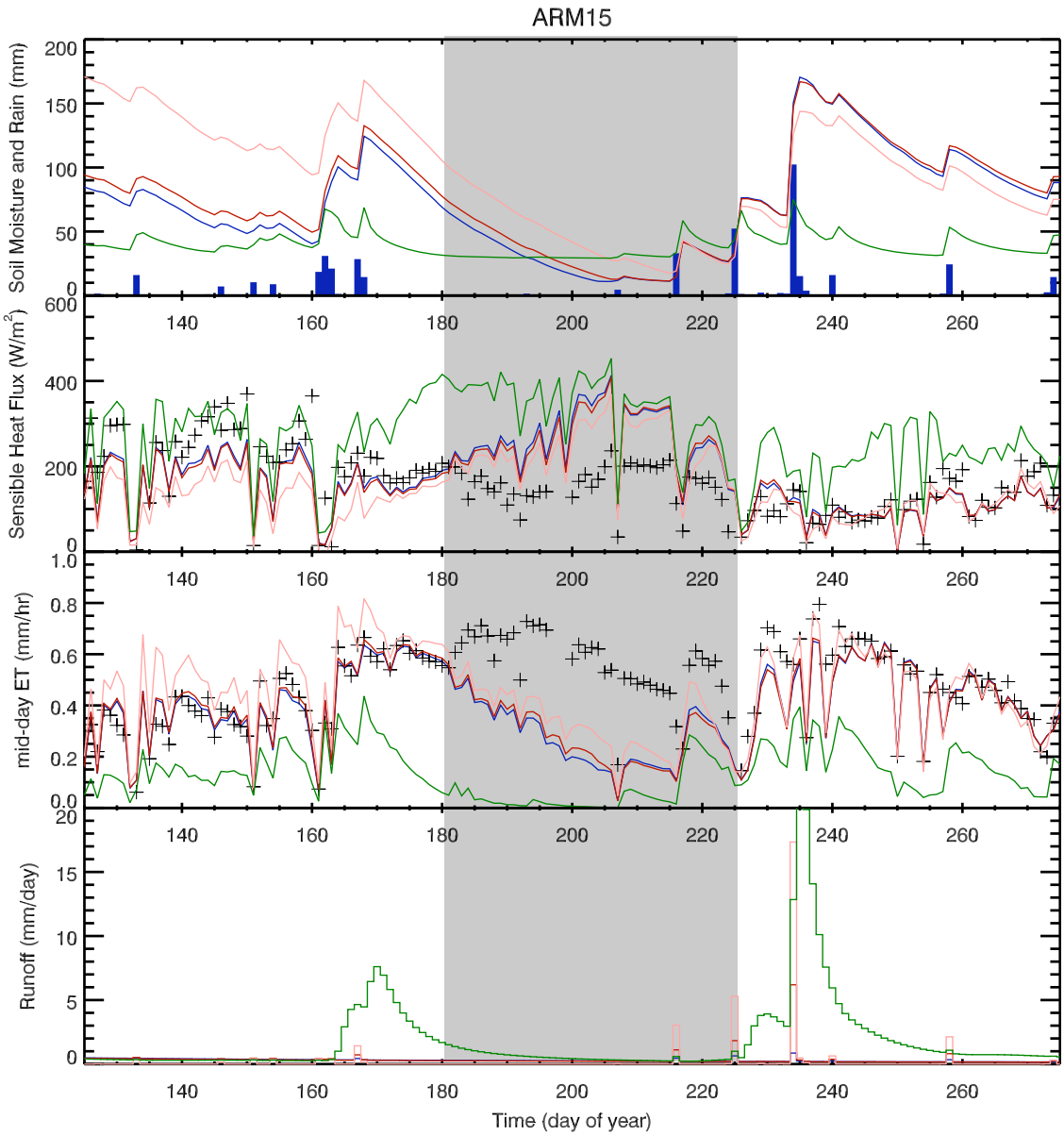

Figure 3. Site details for ARM site E15, as in Figure 2. The ARM forcing data around day 180 appear to be missing a substantial rainstorm. As a result, the observed and modeled ET and SH are inconsistent from day 180 to day 225 (shaded), so this period has been removed from analysis.

at individual sites ranged from −66 to 46 W/m^2 for the MODIS-derived model and from −141 to 35 W/m^2 for the texture model.

[44] A similar pattern is present in the sensible heat flux results. The average SH error for the MODIS-derived model was 61 W/m^2 and the bias was 8 W/m^2. The average SH error for the optimal model was 49 W/m^2 and the bias was 6.5 W/m^2. The average SH error for the texture model was 78 W/m^2 and the bias was 39 W/m^2.

[45] These results demonstrate a substantial improvement to the Noah land-surface model when we use remotely sensed surface temperature to determine LHPs compared to using the default texture class average LHPs. This experiment used local observations of surface meteorological data and performed the calibration for the same time period that was used for the verification (2005).

[46] In addition, we found that the MODIS-derived model performed better than models calibrated using locally observed surface temperatures. When using locally observed surface temperature we calculated an average LH error of 76 W/m^2 at a similar set of ARM sites in addition to nine sites from the International H2O Project (IHOP). The IHOP sites are the in the same region as the ARM sites. This LH error is higher than the MODIS-derived model LH error of 67 W/m^2. These results suggest that the local observations of surface temperature are not as useful for determining larger scale LHPs. This is probably because the local observations of surface temperature (≈4 m^2) may not be representative of the area over which the latent and sensible heat fluxes are observed (≈0.1 km^2). The larger scale MODIS surface temperatures (1 km^2) used in this study appear better representative of the larger scale hydraulic processes.

Table 3. Latent Heat Flux Summary Statistics for Each Model Experiment[a]

	LHP_{opt}		LHP_{af}		LHP_{hf}		LHP_{txt}	
Site	RMSE	Bias	RMSE	Bias	RMSE	Bias	RMSE	Bias
ARM 1*	89	−44	74	5			86	3
ARM 3	56	4	77	40			68	30
ARM 4	36	6	69	46			53	−36
ARM 5*	85	−22	101	−15			100	35
ARM 6	61	19	56	−15			65	12
ARM 7	45	−3	47	−19	53	5	85	−60
ARM 8	41	−6	76	−63	42	−2	99	−84
ARM 9	62	3	71	21	71	−6	106	−64
ARM 13*	71	−9	117	−95	101	−70	105	−79
ARM 15	35	−10	36	−8	53	19	160	−141
ARM 20	47	−5	88	−66			117	−93
ARM 21*	85	1	108	44			102	−17
ARM 24	55	−4	82	25			61	16
ARM 27	47	−12	47	−12			114	−78
Subset	50.4	−0.9	66.9	−6.4	56.8	3.5	97.8	−50.2
All Data	58.2	−5.8	74.9	−8.0			94.4	−39.7

[a]RMSE and bias summaries for all data are given at the bottom of each column. Sites with an asterisk are not included in the subset summaries as explained in the text.

[47] While sites E1, 5, 13, and 21 may have worked poorly because of measurement errors, it is worth examining the relationship between these sites and their associated land cover type. There was only one site in this study that was a forest (E21), and our methodology did not appear to work at that site. There are two primary reasons that we suspect for this. The first is that the dense vegetation cover limits the effect of SHPs on latent heat fluxes as found by *Gutmann and Small* [2007], and thus calibrating SHPs has little effect on the model. The second is that the observed LH at this site may be influenced by Okmulgee Lake, which is approximately 500 m away. The lake may be inside of the flux tower footprint at times because the flux tower at site E21 is higher than at other sites. Evaporation from the lake surface and groundwater accessed by tree roots could both substantially change the local fluxes, and Noah does not include a groundwater component. Conversely, the lake may be included in the 1 km MODIS pixel, thus changing the surface temperature that we are using to derive LHPs. Both of these effects would fit with the observed model biases for this site. The texture class model is biased too low, consistent with enhanced latent heat flux at this site as a result of local groundwater. The MODIS-derived LHP model is biased too high, consistent with a model fit to surface temperatures that are too cool.

[48] The remaining three bad sites are harder to explain. There was also only one site that was largely barren of vegetation cover (E1), and our methodology did not appear to work at this site either. The LH error at this site actually improved with the LHP_{af} when compared to both the LHP_{txt} and the LHP_{opt}, but even the LHP_{opt} had a substantial LH error. This implies that errors in other parameters in the model or in the observed LH or forcing data may be more important at this site. One possibility is that the Noah bare soil evaporation parameter (FXEXP) may need to be calibrated as found by *Peters-Lidard et al.* [2008]. It is possible that this is also the reason why sites E5 and E13 did not perform well. These sites had mean vegetation covers of 40% and 35% respectively, lower than any of the sites that appeared to work well except for site E8 (30%), and it is possible that the default value for FXEXP happens to work well at site E8.

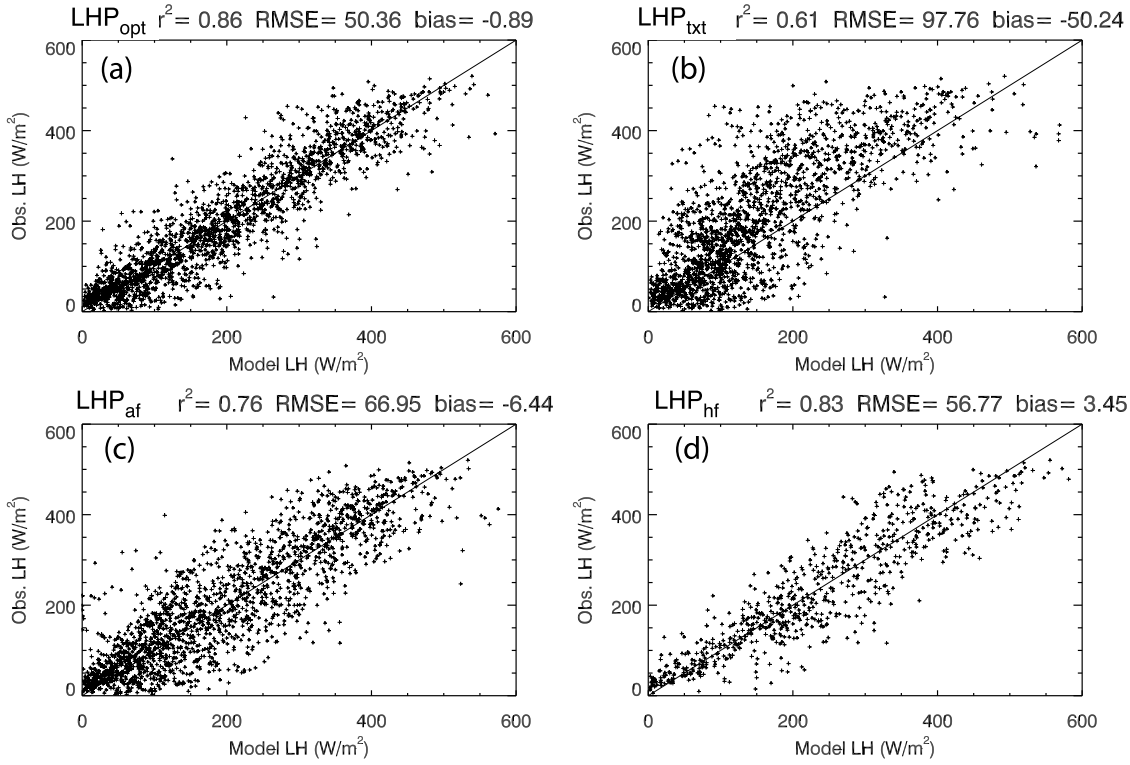

Figure 4. Modeled vs. measured midday latent heat flux for the (a) LHP_{opt}, (b) LHP_{txt}, (c) LHP_{af}, and (d) LHP_{hf}. Ordinary least squares r^2, root mean square error, and bias are on top of each graph.

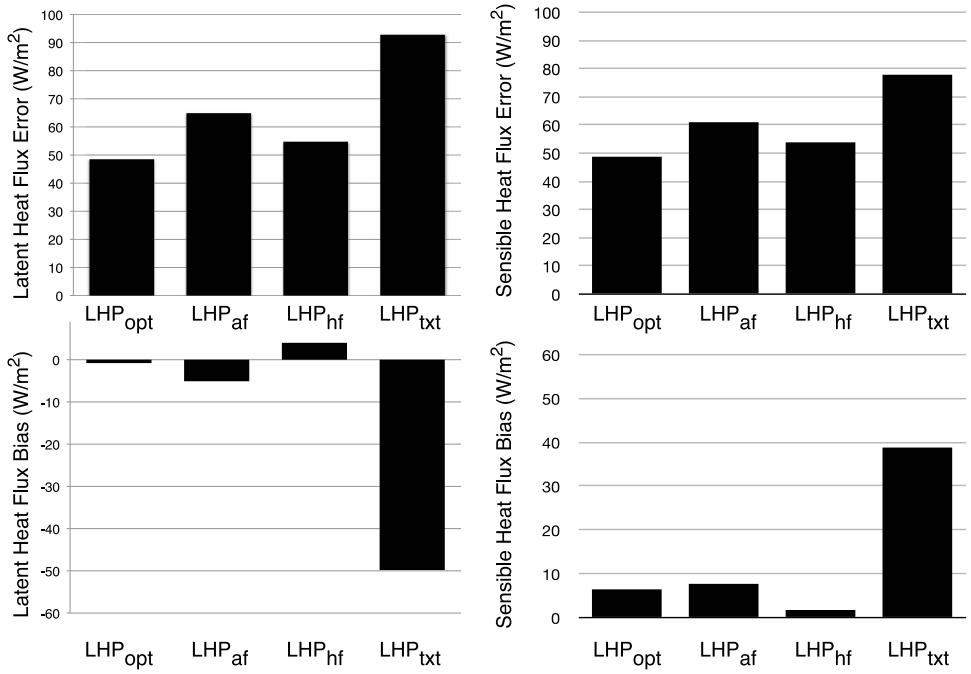

Figure 5. (left) Latent and (right) sensible (top) heat flux root mean square errors and (bottom) bias averaged across all sites for the optimal LHP model (LHP_{opt}), the two MODIS-derived LHP models (LHP_{af}, LHP_{hf}) and the texture class-derived LHP model (LHP_{txt}).

3.2. Experiment 2: HRLDAS Forcing Data

[49] Results for experiment two are presented in Table 3 and Figures 4 and 5. We use the same methodology to subset the sites as we did in experiment 1. The sites are E7, 8, 9, and 15. The average midday LH error for the HRLDAS forced model is 56 W/m^2 and the bias is 3.5 W/m^2. The average midday SH error for the HRLDAS forced model is 54 W/m^2 and the bias is −2.0 W/m^2. This is actually slightly better than the performance of the ARM forced model. When we look at the same four sites with the optimal, ARM forced, and texture models we see LH errors of 48, 61, and 115 W/m^2, and biases of −3.8, 3.5, and −86 W/m^2 respectively. For these four sites, the HRLDAS forced model performs better than the ARM forced model. Similarly, the errors in sensible heat flux for the HRLDAS forced model were better with an error of 54 W/m^2 and a bias of 2 W/m^2.

[50] These results show that we do not need local observations of meteorological data to use as input to the Noah land-surface model. Using the HRLDAS forcing data instead of the locally observed forcing data appears to improve the predicted LHPs. It is unclear if these results will be consistent when we examine a larger number of sites. A regional forcing data set may be better to use because local meteorological observations will have missing data periods. Precipitation has been shown to be a very important forcing parameter for inverse modeling in particular [*Peters-Lidard et al.*, 2008], and a missing precipitation observation will substantially deteriorate model performance. The HRLDAS forcing data set may be less likely to completely miss a precipitation event. In addition, local observations are representative of micrometeorological conditions that may not be the same as those over the larger area covered by a satellite or flux tower footprint.

[51] This experiment also showed that the LHPs derived from surface temperature are not specific to the calibration period used. The HRLDAS forcing data and MODIS surface temperatures used for calibration in this experiment were for the time period January 2002 to June 2002 and were verified during 2005. Because the HRLDAS forced model LH is similar to the observed fluxes for this period, we gain confidence that the LHPs derived are specific to the area being studied rather than to the calibration period.

3.3. Experiment 3: Model Sensitivity

[52] Results for experiment three are presented in Figures 6 and 7. For this experiment, LHPs were derived using observed ARM forcing data and MODIS surface temperature observations (LHP_{af}). We present optimal, MODIS derived, and texture based model results with variations in the model albedo, roughness length, and minimum canopy resistance. At ARM site E9, with variations in albedo from 0.1 to 0.26 (observed = 0.2) LH error varied from 62 to 68 W/m^2 for the optimal model, 65 to 73 W/m^2 for the MODIS-derived model, and 98 to 102 W/m^2 for texture based model (Figure 6, top). With variations in roughness length from 0.005 to 0.5 m (default = 0.05) LH error varied from 64 to 65 W/m^2 for the optimal model, 67 to 69 W/m^2 for the MODIS-derived model, and 97 to 98 W/m^2 for texture based model (Figure 6, middle). At ARM site E15, with variations in minimum canopy resistance from 30 to 70 s/m (default = 40 s/m), LH error varied from 46 to 50 W/m^2 for the optimal model, 44 to 46 W/m^2 for the MODIS-derived model, and 146 to 172 W/m^2 for texture based (Figure 6, bottom).

[53] We do not focus on SH in this study because SH is less sensitive to SHPs [*Bastidas et al.*, 1999]; however, we

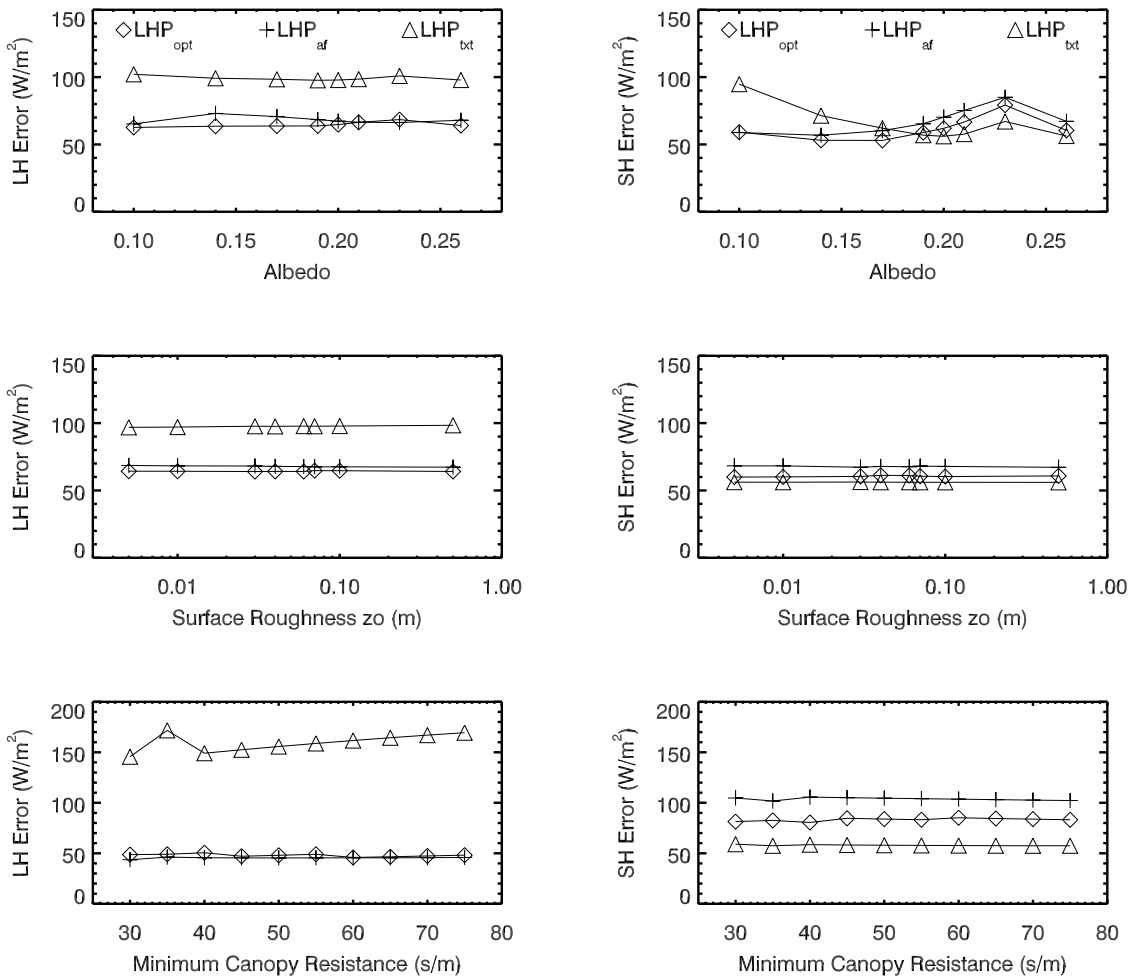

Figure 6. Root mean square error in (left) latent and (right) sensible heat flux for (diamonds) LHP_{opt}, (+) LHP_{af}, and (Δ) LHP_{txt} for site E9 as a function of varying (top) albedo, (middle) roughness length (z_o), and for site E15 as a function of (bottom) minimum canopy resistance, R_s.

note a few important points here. The SH errors are also generally insensitive to errors in other model parameters, with the exception of albedo (Figure 6). Albedo plays a large role in the surface energy balance, and as such large changes to it must change other terms in the surface energy balance. Here, SH errors vary more as a function of albedo than they do as a function of LHP parameter set. For roughness length and minimum canopy resistance, SH errors show less change between parameter sets than LH errors do.

[54] In addition, it is worth pointing out that SH errors are actually lower for the LHP_{txt} model than for the other models at these two sites (as previously shown, this is not the case across all sites.) This is not because the LHP_{opt} and LHP_{af} models perform particularly poorly at these sites, although they are worse than the average, but because the LHP_{txt} happens to perform well in predicting SH at these sites. LHP_{txt} SH errors at these sites are just over 50 W/m^2, while the average SH error across all sites for the LHP_{txt} model is 78 W/m^2.

[55] For all of the sensitivity tests, the LH error varied more between different LHP methods than it did as a function of errors in other model parameters. This could suggest that the inversely derived LHPs (both LHP_{opt} and LHP_{af}) are compensating for these errors. However, an analysis of the derived LHPs suggests that these LHPs are not varying significantly (Figure 7). In all cases, the derived LHP_{af} parameters varied little as a function of errors in other parameters. The derived LHP_{opt} only varied by about 10% of the range used in the inverse procedure as a result of variations in albedo. The LHP_{opt} Ks parameter was the most sensitive parameter in these tests, and it varied from 70–500 cm/d when very large errors in albedo were introduced. This is substantially smaller than the total variation in the SHP database of *Schaap and Leij* [1998], in which measured K_s values vary from 0.05 to 20000 cm/d. Varying the roughness length from 0.05 to 0.5 m (Figure 7) had very little effect on K_s and m in both the LHP_{opt} and the LHP_{af}. LHP_{opt} K_s varied from 70 to 120 cm/d and m varied from 0.16 to 0.19.

[56] For the minimum canopy resistance test, there is a step change in LHP_{opt} parameters between minimum canopy resistance values of 50 and 55 s/m. In this case, m decreased from 0.34 to 0.19 and K_s increased from 60 to 1100 cm/d. These parameters have opposite impacts on the net effect of SHPs. The decrease in m causes the unsaturated conductivity to decrease more rapidly as moisture content decreases. This decrease may compensate for the higher saturated conductivity. Indeed, *Gutmann and Small* [2007] showed that at a

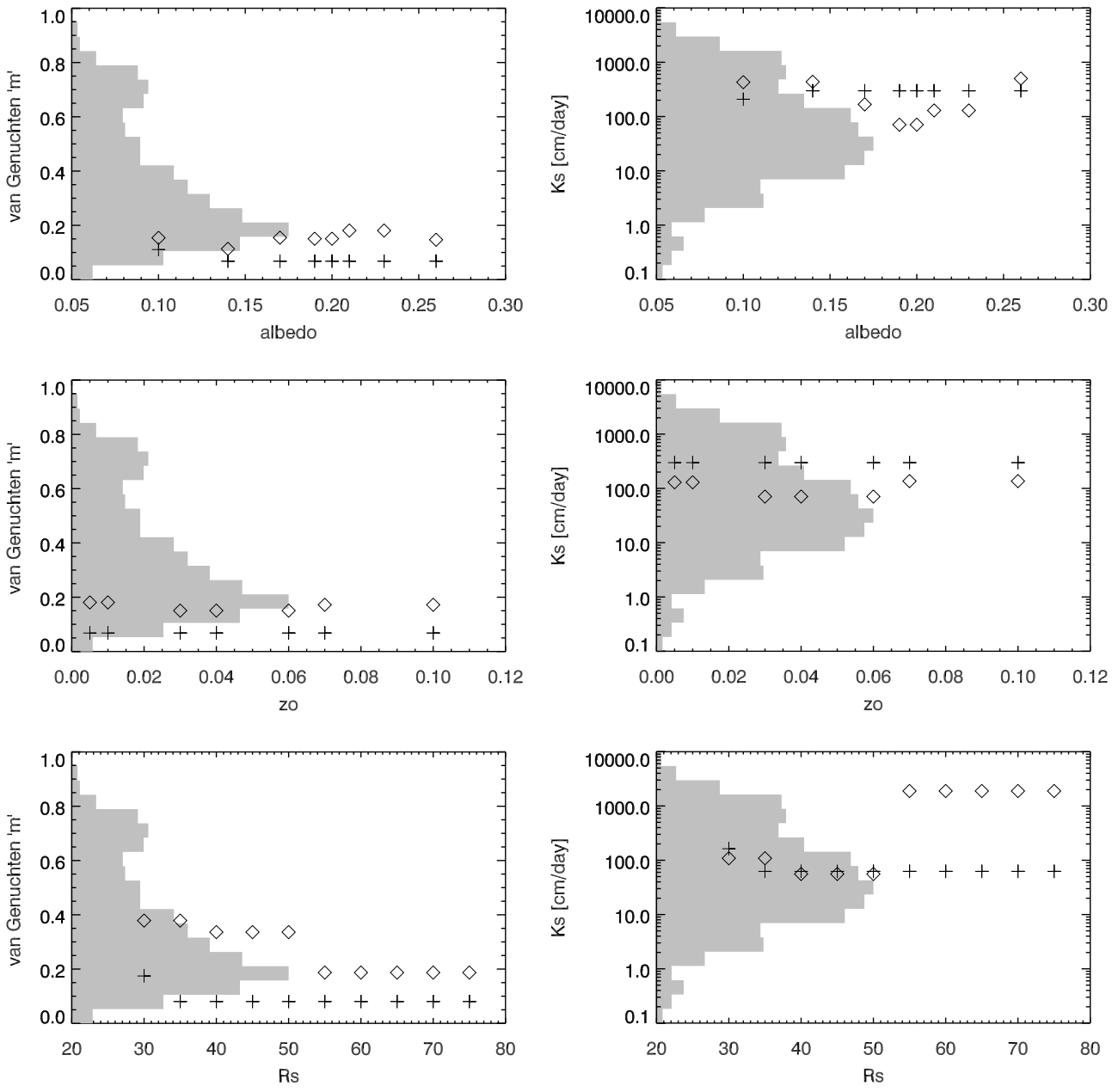

Figure 7. (right) K_s and (left) van Genuchten m for (diamonds) LHP_{opt} and (+) LHP_{af} for site E9 as a function of varying (top) albedo and (middle) z_o and for site E15 as a function of (bottom) R_s. For reference, histograms of these parameters from the database of *Schaap and Leij* [1998] are displayed as well. K_s is consistently higher than the mean of the distribution and m is typically lower than the mean of the distribution.

site with 60% vegetation cover, a decrease in m from 0.34 to 0.19 would increase modeled LH by ≈50 W/m^2, while an increase in K_s from 60 to 1100 cm/d would decrease modeled LH by ≈80 W/m^2. This indicates that the individual parameters are not necessarily stable in all conditions but that the effective hydraulic conductivity curves are stable. Extremes in vegetation type (tundra, some forests) can reach values as high as 150 s/m in the default Noah parameter set. It is possible to reach larger minimum canopy resistance values in more arid shrublands (300 s/m), and future tests should probably expand this experiment to higher values. Indeed, recent work has shown that the minimum canopy resistance of grasses can vary substantially over time even at a single site [*Alfieri et al.*, 2008].

[57] These results show that the inverse procedure is relatively insensitive to substantial errors in three other important model parameters. The three parameters we varied control the energy available to the model (albedo), the turbulent exchange between the land surface and the atmosphere (roughness length), and the transpiration rate (minimum canopy resistance). We showed that even when varying these parameters by more than the likely error in each, both the derived LHPs and the resultant LH error were largely insensitive to these errors. It should be noted that we varied

each of these parameters independently, and thus we do not know the effect of interactions between these parameters. In addition, the simplicity of the inverse procedure does not allow an estimation of the errors in derived LHPs, or a more sophisticated analysis of the importance of each parameter. Furthermore, our results will not be applicable to parameter errors outside of the range we tested here.

4. Conclusions

[58] We have shown that using MODIS observations of surface temperature to derive landscape hydraulic properties decreases error in modeled latent and sensible heat fluxes by over 60% compared with standard texture based classifications. More importantly, model runs using LHPs derived from remotely sensed surface temperature removed 90% of the bias between modeled and observed latent heat fluxes when the bias is averaged across multiple sites. This result holds even when locally measured meteorological data are not available. We have also shown that these model parameters are persistent through time; LHPs calibrated in 2002, improve model fluxes for 2005.

[59] Furthermore, we have shown that the calibration of these parameters is not sensitive to substantial perturbations to other model parameters. Varying albedo from 0.1 to 0.26, surface roughness from 0.005 to 0.5 m, and minimum canopy resistance from 30 to 75 s/m had a minimal impact on both the LHP parameter values and on the errors in modeled latent and sensible heat fluxes. The exceptions to this are that changes in albedo affected sensible heat flux errors in all models, and minimum canopy resistance affected the errors in the LHP_{txt} model and the parameter values in the LHP_{opt} model. This suggests that the LHPs derived in this study are not compensating for errors in other model parameters. One concern is that when varying the minimum canopy resistance, the LHP_{opt} model saturated conductivity and the van Genuchten "m" parameter both shifted, but they changed in such a way as to cancel the effect of the shift in the other. This suggests that while the effective value of the LHPs may be stable across model runs and parameters, the individual LHP parameters derived may not always be stable. The simplicity of the inverse procedure and sensitivity analysis limits our ability to infer anything about interactions between parameters or to directly estimate an error for the derived LHPs.

[60] It is not clear that the LHPs derived through this procedure are directly related to the SHPs at the individual sites. No ground observations of SHPs are available, and texture is not an adequate method of predicting SHPs for comparison purposes [*Gutmann and Small*, 2005]. The LHPs derived here do appear to improve the model representation of the local hydrology, as such, they could be used to learn about larger-scale hydraulic processes at these sites. However, future work must address the relationship between inversely derived LHPs and field observed SHPs first.

[61] This study may have global applications, but first a better assessment of its strengths and weaknesses will be required. The present study analyzed sites with a variety of land cover types. While it is difficult to draw any clear conclusions from the limited number of sites, a few relationships are worth noting. This study does not appear to work well at heavily vegetated sites (E21) or nearly bare sites (E1). It is possible that these sites were problematic because of measurement errors, but it is also possible that high vegetation cover fractions inhibit the SHP inversion as suggested by *Gutmann and Small* [2007]. Similarly, site E1 may not work well because of measurement errors or because at nearly bare sites, the model parameter FXEXP becomes more important than SHPs as suggested by *Peters-Lidard et al.* [2008].

[62] Finally, these specific LHPs are only valid at the sites they were derived for with the model that was used to derive them. We do not know if these LHPs would work in another model, future work should address the transferability of these parameters to other models. We would also like to see these LHPs used in a coupled WRF-Noah model to analyze the impact of the modified LHPs on weather forecasts.

[63] **Acknowledgments.** The National Center for Atmospheric Research is supported by the National Science Foundation. This research was partially supported by NNG04GO83G (CU Boulder) from the NASA Earth Science Enterprise (program manager J. Entin). ARM data were obtained from the Atmospheric Radiation Measurement (ARM) Program sponsored by the U.S. Department of Energy, Office of Science, Office of Biological and Environmental Research, Environmental Sciences Division. We gratefully acknowledge the three anonymous reviewers and the associate editor who helped improve this manuscript.

References

Alfieri, J. G., D. Niyogi, P. D. Blanken, F. Chen, M. A. LeMone, K. E. Mitchell, M. B. Ek, and A. Kumar (2008), Estimation of the minimum canopy resistance for croplands and grasslands using data from the 2002 international H2O project, *Mon. Weather Rev.*, *136*(11), 4452–4469, doi:10.1175/2008MWR2524.1.

Arya, L., F. Leij, M. van Genuchten, and P. Shouse (1999), Scaling parameter to predict the soil water characteristic from particle-size distribution data, *Soil Sci. Soc. Am. J.*, *63*, 510–519.

Bastidas, L., H. Gupta, S. Sorooshian, W. Shuttleworth, and Z. Yang (1999), Sensitivity analysis of a land surface scheme using multicriteria methods, *J. Geophys. Res.*, *104*(D16), 19,481–19,490.

Bedford, D. R., and E. E. Small (2008), Spatial patterns of ecohydrologic properties on a hillslope-alluvial fan transect, central new mexico, *Catena*, *73*(1), 34–48, doi:10.1016/j.catena.2007.08.005.

Betts, A. K., J. H. Ball, M. Bosilovich, P. Viterbo, Y. C. Zhang, and W. B. Rossow (2003), Intercomparison of water and energy budgets for five mississippi subbasins between ecmwf reanalysis (era-40) and nasa data assimilation office fvgcm for 1990–1999, *J. Geophys. Res.*, *108*(D16), 8618, doi:10.1029/2002JD003127.

Bonan, G., D. Pollard, and S. Thompson (1993), Influence of subgrid-scale heterogeneity in leaf area index, stomatal resistance, and soil moisture on grid-scale land-atmosphere interactions, *J. Clim.*, *6*(10), 1882–1897.

Bonan, G., K. Oleson, M. Vertenstein, S. Levis, X. Zeng, Y. Dai, R. Dickinson, and Z. Yang (2002), The land surface climatology of the community land model coupled to the ncar community climate model, *J. Clim.*, *15*, 3123–3149.

Boulet, G., A. Chehbouni, P. Gentine, B. Duchemin, J. Ezzahar, and R. Hadria (2007), Monitoring water stress using time series of observed to unstressed surface temperature difference, *Agric. For. Meteorol.*, *146*, 159–172.

Burke, E., R. Gurney, L. Simmonds, and P. O'neill (1998), Using a modeling approach to predict soil hydraulic properties from passive microwave measurements, *IEEE Trans. Geosci. Remote Sens.*, *36*, 454–462.

Chauhan, N., S. Miller, and P. Ardanuy (2003), Spaceborne soil moisture estimation at high resolution: a microwave-optical/ir synergistic approach, *Int. J. Remote Sens.*, *24*(22), 4599–4622, doi:10.1080/0143116031000156837.

Chen, F., and J. Dudhia (2001), Coupling an advanced land surface-hydrology model with the Penn State-NCAR MM5 modeling system. Part I: Model implementation and sensitivity, *Mon. Weather Rev.*, *129*, 569–585.

Chen, F., Z. Janjic, and K. Mitchell (1997), Impact of atmospheric surface-layer parameterizations in the new land-surface scheme of the ncep mesoscale eta model, *Boundary Layer Meteorol.*, *85*, 391–421.

Chen, F., et al. (2007), Description and evaluation of the characteristics of the ncar high-resolution land data assimilation system, *J. Appl. Meteorol. Clim.*, *46*, 694–713, doi:10.1175/JAM2463.1.

Duan, Q., et al. (2006), Model parameter estimation experiment (MOPEX): An overview of science strategy and major results from the second and third workshops, *J. Hydrol.*, *320*, 3–17.

Eching, S., J. Hopmans, and W. Wallender (1994), Estimation of in-situ unsaturated soil hydraulic functions from scaled cumulative drainage data, *Water Resour. Res.*, *30*, 2387–2394.

Ek, M., K. Mitchell, Y. Lin, E. Rogers, P. Grunmann, V. Koren, G. Gayno, and J. Tarpley (2003), Implementation of Noah land surface model advances in the National Centers for Environmental Prediction operational mesoscale eta model, *J. Geophys. Res.*, *108*(D22), 8851, doi:10.1029/2002JD003296.

Feddes, R., M. Menenti, P. Kabat, and W. Bastiaanssen (1993), Is large-scale inverse modeling of unsaturated flow with areal average evaporation and surface soil-moisture as estimated from remote-sensing feasible, *J. Hydrol.*, *143*, 125–152.

Friedl, M. (1996), Relationships among remotely sensed data, surface energy balance, and area-averaged fluxes over partially vegetated land surfaces, *J. Appl. Meteorol.*, *35*, 2091–2103.

Gillies, R. R., and T. N. Carlson (1995), Thermal remote sensing of surface soil water content with partial vegetation cover for incorporation into climate models, *J. Appl. Meteorol.*, *34*, 745–756.

Gutman, G., and A. Ignatov (1998), The derivation of green vegetation fraction from noaa/avhrr data for use in numerical weather prediction models, *Int. J. Remote Sens.*, *19*, 1533.

Gutmann, E., and E. Small (2005), The effect of soil hydraulic properties vs. soil texture in land surface models, *Geophys. Res. Lett.*, *32*(2), L02402, doi:10.1029/2004GL021843.

Gutmann, E., and E. Small (2007), A comparison of land surface model soil hydraulic properties estimated by inverse modeling and pedotransfer functions, *Water Resour. Res.*, *43*, W05418, doi:10.1029/2006WR005135.

Hoffmann-Riem, H., M. van Genuchten, and H. Fluhler (1999), A general model of the hydraulic conductivity of unsaturated soils, in *Proceedings of the International Workshop, Characterization and Measurements of the Hydraulic Properties of Unsaturated Porous Media*, edited by M. van Genuchten, F. Leij, and L. Wu, pp. 31–42, University of California, Riverside.

Hogue, T., L. Bastidas, H. Gupta, S. Sorooshian, K. Mitchell, and W. Emmerich (2005), Evaluation and transferability of the noah land surface model in semiarid environments, *J. Hydrometeorol.*, *6*(1), 68–84.

Huete, A., C. Justice, and H. Liu (1994), Development of vegetation and soil indices for MODIS-EOS, *Remote Sens. Environ.*, *49*(3), 224–234.

Jacquemin, and Noilhan (1990), Sensitivity study and validation of a land surface parameterization using the hapex-mobilhy data set, *Boundary Layer Meteorol.*, *52*, 93–134.

Kabat, P., A. Dolman, and J. Elbers (1997), Evaporation, sensible heat and canopy conductance of fallow savannah and patterned woodland in the sahel, *J. Hydrol.*, *189*(1–4), 494–515.

Kollet, S. J., and R. M. Maxwell (2008), Capturing the influence of groundwater dynamics on land surface processes using an integrated, distributed watershed model, *Water Resour. Res.*, *44*(2), W02402, doi:10.1029/2007WR006004.

Koster, R. D., et al. (2004), Regions of strong coupling between soil moisture and precipitation, *Science*, *305*(5687), 1138–1140.

Kurc, S., and E. Small (2004), Dynamics of evapotranspiration in semiarid grassland and shrubland ecosystems during the summer monsoon season, central New Mexico, *Water Resour. Res.*, *40*, W09305, doi:10.1029/2004WR003068.

Leij, F., W. Alves, M. van Genuchten, and J. Williams (1996), Unsaturated soil hydraulic database, UNSODA 1.0 user's manual, *EPA Report EPA/600/R96/095*, U.S. Environmental Protection Agency, Ada, OK.

Leij, F., W. Russell, and S. Lesch (1997), Closed-form expressions for water retention and conductivity data, *Ground Water*, *35*, 848–858.

LeMone, M., F. Chen, M. Tewari, J. Dudhia, B. Geerts, Q. Miao, R. L. Coulter, and R. L. Grossman (2009), Simulating the IHOP_2002 fair-weather CBL with the WRF-ARW-Noah modeling system, part 1: Surface fluxes and CBL structure and evolution along the eastern track, *Mon. Weather Rev.*, Early Online Access, doi:10.1175/2009MWR3003.1.

LeMone, M. A., M. Tewari, F. Chen, J. G. Alfieri, and D. Niyogi (2008), Evaluation of the noah land surface model using data from a fair-weather IHOP_2002 day with heterogeneous surface fluxes, *Mon. Weather Rev.*, *136*(12), 4915–4941, doi:10.1175/2008MWR2354.1.

Leung, L. R., Y.-H. Kuo, and J. Tribbia (2006), Research needs and directions of regional climate modeling using WRF and CCSM, *Bull. Am. Meteorol. Soc.*, *87*, 1747–1751, doi:10.1175/BAMS-887-12-1747.

Maayar, M. E., and J. Chen (2006), Spatial scaling of evapotranspiration as affected by heterogeneities in vegetation, topography, and soil texture, *Remote Sens. Environ.*, *102*(1–2), 33–51, doi:10.1016/j.rse.2006.01.017.

Montandon, L., and E. Small (2008), The impact of soil reflectance on the quantification of the green vegetation fraction from NDVI, *Remote Sens. Environ.*, *112*(4), 1835–1845.

Nachabe, M. (1995), Estimating hydraulic conductivity for models of soils with macropores, *J. Irrig. Drain. Eng.*, *121*, 95–102.

Pauwels, V. R. N., A. Balenzano, G. Satalino, H. Skriver, N. E. C. Verhoest, and F. Mattia (2009), Optimization of soil hydraulic model parameters using synthetic aperture radar data: An integrated multidisciplinary approach, *IEEE Trans. Geosci. Remote Sens.*, *47*(2), 455–467, doi:10.1109/TGRS.2008.2007849.

Peters-Lidard, C. D., D. M. Mocko, M. Garcia, J. A. Santanello, M. A. Tischler, M. S. Moran, and Y. Wu (2008), Role of precipitation uncertainty in the estimation of hydrologic soil properties using remotely sensed soil moisture in a semiarid environment, *Water Resour. Res.*, *44*(5), W05S18, doi:10.1029/2007WR005884.

Poulsen, T., P. Moldrup, T. Yamaguchi, and O. Jacobsen (2000), Predicting saturated and unsaturated hydraulic conductivity in undisturbed soils from soil water characteristics, *Soil Sci.*, *164*, 877–887.

Reynolds, C., T. Jackson, and W. Rawls (1999), Estimated available water content from the fao soil map of the world, global soil profile databases, pedo-transfer functions, *Tech. Rep.* http://www.ngdc.noaa.gov/seg/fliers/se-2006.shtml, Published by the NOAA National Geophysical Data Center, Boulder, CO.

Santanello, J., C. Peters-Lidard, M. Garcia, D. Mocko, M. Tischler, M. Moran, and D. Thoma (2007), Using remotely-sensed estimates of soil moisture to infer soil texture and hydraulic properties across a semi-arid watershed, *Remote Sens. Environ.*, *110*, 79–97.

Schaap, M., and F. Leij (1998), Database-related accuracy and uncertainty of pedotransfer functions, *Soil Sci.*, *163*, 765–779.

Schaap, M., F. Leij, and M. van Genuchten (2001), Rosetta: A computer program for estimating soil hydraulic parameters with hierarchical pedotransfer functions, *J. Hydrol.*, *251*, 163–176.

Sellers, P., D. Randall, G. Collatz, J. Berry, C. Field, D. Dazlich, C. Zhang, G. Collelo, and L. Bounoua (1996), A revised land surface parameterization (SiB2) for atmospheric GCMs part I: Model formulation, *J. Clim.*, *9*, 676–705.

Seneviratne, S. I., D. Luethi, M. Litschi, and C. Schaer (2006), Land-atmosphere coupling and climate change in europe, *Nature*, *443*, 205–209, doi:10.1038/nature05095.

Simunek, J., and M. vanGenuchten (1997), Estimating unsaturated soil hydraulic properties from multiple tension disc infiltrometer data, *Soil Sci.*, *162*, 383–398.

Soet, M., and J. Stricker (2003), Functional behaviour of pedotransfer functions in soil water flow simulation, *Hydrol. Processes*, *17*, 1659–1670.

Stieglitz, M., D. Rind, J. Famiglietti, and C. Rosenzweig (1997), An efficient approach to modeling the topographic control of surface hydrology for regional and global climate modeling, *J. Clim.*, *10*(1), 118–137.

Stoeckli, R., P. L. Vidale, A. Boone, and C. Schaer (2007), Impact of scale and aggregation on the terrestrial water exchange: Integrating land surface models and Rhone catchment observations, *J. Hydrometeorol.*, *8*(5), 1002–1015, doi:10.1175/JHM613.1.

Stolte, J., J. Freijer, W. Bouten, C. Dirksen, J. Halbertsma, J. Vandam, J. Vandenberg, G. Veerman, and J. Wosten (1994), Comparison of 6 methods to determine unsaturated soil hydraulic conductivity, *Soil Sci. Soc. Am. J.*, *58*, 1596–1603.

Twine, T., W. Kustas, J. Norman, D. Cook, P. Houser, T. Meyers, J. Prueger, P. Starks, and M. Wesely (2000), Correcting eddy-covariance flux underestimates over a grassland, *Agric. For. Meteorol.*, *103*, 279–300.

Vandam, J., J. Stricker, and P. Droogers (1992), Inverse method for determining soil hydraulic functions from one-step outflow experiments, *Soil Sci. Soc. Am. J.*, *56*, 1042–1050.

van Genuchten, M. (1980), A closed-form equation for prediction of the hydraulic properties of unsaturated soils, *Soil Sci. Soc. Am. J.*, *44*, 892–898.

van Verseveld, W. J., J. J. McDonnell, and K. Lajtha (2009), The role of hillslope hydrology in controlling nutrient loss, *J. Hydrol.*, *367*(3–4), 177–187, doi:10.1016/j.jhydrol.2008.11.002.

Vrugt, J., G. Schoups, J. Hopmans, C. Young, W. Wallender, T. Harter, and W. Bouten (2004), Inverse modeling of large-scale spatially distrib-

uted vadose zone properties using global optimization, *Water Resour. Res.*, *40*, W06503, doi:10.1029/2003WR002706.

Wan, Z., and J. Dozier (1996), A generalized split-window algorithm for retrieving land-surface temperature from space, *IEEE Trans. Geosci. Remote Sens.*, *34*, 892–905.

Wan, Z., Y. Zhang, and Q. Zhang (2004), Quality assessment and validation of the modis global land surface temperature, *Int. J. Remote Sens.*, *25*(1), 261–274.

Wetzel, P. J., and J.-T. Chang (1987), Concerning the relationship between evapotranspiration and soil moisture, *J. Clim. Appl. Meteorol.*, *26*(1), 18–27.

Zhu, J., and B. Mohanty (2003), Effective hydraulic parameters for steady state vertical flow in heterogeneous soils, *Water Resour. Res.*, *39*(8), 1227, doi:10.1029/2002WR001831.

Zilitinkevich, S. (1995), Non-local turbulent transport: Pollution dispersion aspects of coherent structure of convective flows, in *Air Pollution III - Volume I. Air Pollution Theory and Simulation*, vol. 1, edited by H. Power, N. Moussiopoulos, and C. Brebbia, pp. 53–60, Computational Mechanics Publications.

E. D. Gutmann, National Center for Atmospheric Research, PO Box 3000, Boulder, CO 80305-5602, USA. (gutmann@ucar.edu)

E. E. Small, Department of Geological Sciences, University of Colorado at Boulder, UCB 399, 2200 Colorado Ave., Boulder, CO 80309-0399, USA.